

Thinking with Images as Continuous Actions: Numerical Visual Chain-of-Thought

Kesen Zhao¹ Beier Zhu¹✉ Junbao Zhou¹ Xingyu Zhu² Zhongqi Yue³ Hanwang Zhang¹

Abstract

Recent multimodal large language models (MLLMs) increasingly rely on *visual chain-of-thought* to perform region-grounded reasoning over images. However, existing approaches ground regions via either textified coordinates—causing modality mismatch and semantic fragmentation—or fixed-granularity patches that both limit precise region selection and often require non-trivial architectural changes. In this paper, we propose Numerical Visual Chain-of-Thought (NV-CoT), a framework that enables MLLMs to reason over images using *continuous* numerical coordinates. NV-CoT expands the MLLM action space from discrete vocabulary tokens to a continuous Euclidean space, allowing models to directly generate bounding-box coordinates as actions with only minimal architectural modification. The framework supports both supervised fine-tuning and reinforcement learning. In particular, we replace categorical token policies with a Gaussian (or Laplace) policy over coordinates and introduce stochasticity via reparameterized sampling, making NV-CoT fully compatible with GRPO-style policy optimization. Extensive experiments on three benchmarks against eight representative visual reasoning baselines demonstrate that NV-CoT significantly improves localization precision and final answer accuracy, while also accelerating training convergence, validating the effectiveness of continuous-action visual reasoning in MLLMs. The code is available in <https://github.com/kesenzhao/NV-CoT>.

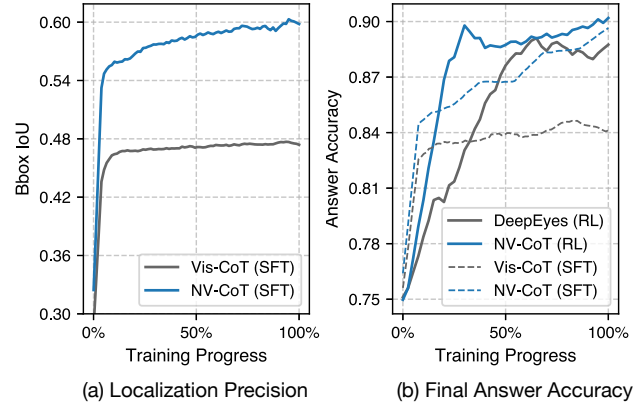


Figure 1. Our NV-CoT outperforms text-based visual CoT models (Vis-CoT (Shao et al., 2024a) and DeepEyes (Zheng et al., 2025)) in **localization precision**, **answer accuracy**, and **convergence speed** across both SFT and RL. SFT-based models are evaluated on the Vis-CoT-363K dataset (Shao et al., 2024a), where ground-truth bounding boxes are available, while RL-based models are evaluated on the DeepEyes-47K dataset (Zheng et al., 2025). We only replace the text-space discrete coordinate objective with our Euclidean-space continuous one, while keeping all other training configurations unchanged for a fair comparison.

1. Introduction

Recent advances in multimodal large language models (MLLMs) have enabled deeper reasoning over visual inputs via “thinking with images” (*i.e.*, visual chain-of-thought) (Zheng et al., 2025; Shao et al., 2024a; Zhao et al., 2025; Li et al., 2025b; Su et al., 2025b). In this paradigm, models first localize task-relevant image regions aligned with the textual query. They then conduct multi-step reasoning by explicitly grounding intermediate inferences on these detected regions. Such region-grounded visual reasoning is a fundamental capability for MLLMs and underpins a broad range of downstream applications.

To align with the text-based output interface, many existing MLLMs (Liu et al., 2025; Bai et al., 2025; Zhu et al., 2025) serialize localized regions as bounding-box coordinates in **text**, *e.g.*, $["x_1", "y_1", "x_2", "y_2"]$, and then invoke a cropping tool to extract the corresponding patch (Figure 2 (a)). Despite its simplicity, this design faces two fundamental issues. (1) Modality mismatch: coordinates are continuous

¹Nanyang Technological University ²Chalmers University of Technology and University of Gothenburg ³University of Science and Technology of China. Correspondence to: Beier Zhu <beier.zhu.94@gmail.com>.

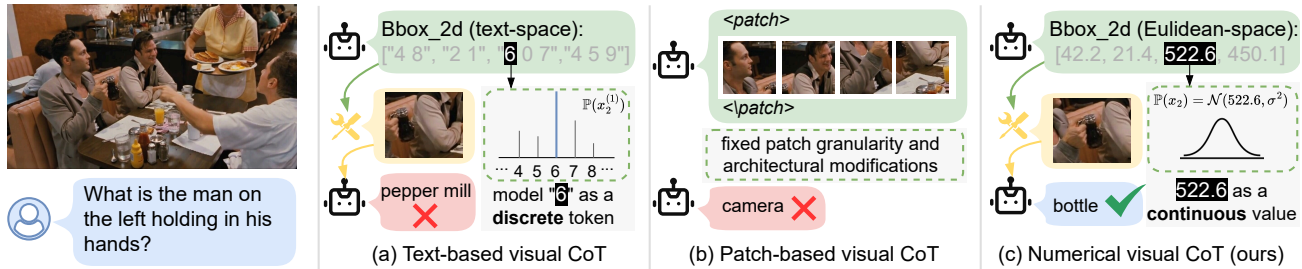


Figure 2. Comparison of different paradigms for thinking with images. (a) Text-based approaches represent localized regions as discrete coordinate tokens, leading to modality mismatch and fragmented semantics. (b) Patch-based approaches reason directly over fine-grained visual tokens but are constrained by the fixed spatial granularity of the vision backbone. (c) Our NV-CoT predicts region coordinates in continuous space, enabling flexible and precise localization.

in the visual world but are predicted as discrete text tokens and typically trained with cross-entropy, which ignores geometric proximity (e.g., predicting $x_1=“3.2”$ may be penalized similarly to $x_1=“4.1”$ when the target is $x_1^*=“3.1”$, since both predictions differ from the target by only a single discrete token under token-level cross-entropy). (2) Semantic fragmentation: numbers are tokenized into multiple unrelated sub-tokens, making numerical comparison and reasoning brittle and prone to hallucination (e.g., confusing whether “3.11” or “3.9” is larger).

Several recent works attempt to alleviate these issues by enabling MLLMs to operate directly on fine-grained visual patches (Figure 2 (b)). For example, LVR (Li et al., 2026) performs reasoning in the visual embedding space, while PaDT (Su et al., 2025a) generates indices corresponding to original visual patch embeddings. Nevertheless, these approaches are fundamentally constrained by the fixed granularity of the vision backbone, as the predefined patch partitioning limits flexible and precise region selection. In addition, patch-generation or patch-indexing mechanisms often require non-trivial architectural changes, which weakens modularity and limits general applicability across MLLMs.

To avoid brittle textified coordinates with only minimal architectural changes, we propose Numerical Visual Chain-of-Thought (NV-CoT), which expands the MLLM action space from discrete vocabulary tokens to a continuous Euclidean space, enabling the model to directly generate numerical bounding box coordinates as actions (Figure 2 (c)). Specifically, we extend the standard LLM head with four coordinate outputs that directly predict the numerical bounding-box coordinates (e.g., $[x_1, y_1, x_2, y_2]^1$). Notably, NV-CoT is applicable to both supervised fine-tuning (SFT) and reinforcement learning (RL) stages. In the SFT stage, we replace token-level cross-entropy with a regression loss to supervise continuous bounding-box coordinates. However, extending this idea to the RL stage is non-trivial. Most

¹We write text-based coordinates as $[“x_1”, “y_1”, “x_2”, “y_2”]$ and numerical coordinates as $[x_1, y_1, x_2, y_2]$.

LLM-oriented policy optimization methods parameterize the policy as a token-level categorical distribution over the vocabulary, which naturally supports discrete actions but does not directly accommodate continuous coordinate outputs. Furthermore, deterministic coordinate prediction lacks the stochasticity required by GRPO-style algorithms for advantage estimation and policy exploration. To address these challenges, we replace the categorical policy with a Gaussian policy that explicitly models continuous coordinate regression. Stochasticity is introduced via the reparameterization trick, where the model predicts both the mean and standard deviation of the bounding box distribution and samples coordinates accordingly. This design enables efficient exploration and stable gradient propagation, while also providing closed-form likelihoods for computing importance ratios and KL regularization, making NV-CoT compatible with GRPO-style RL frameworks. Finally, we also provide a Laplace-policy variant of NV-CoT, motivated by the empirical robustness and favorable performance of ℓ_1 -type losses for localization; it serves as a drop-in replacement for the Gaussian policy under the same GRPO pipeline.

Extensive experiments on V^* Bench (Wu & Xie, 2024), HR-Bench 4K (Wang et al., 2025c), and HR-Bench 8K (Wang et al., 2025c) demonstrate that NV-CoT consistently improves visual reasoning performance. For example, on V^* Bench, NV-CoT-7B outperforms LVR-7B (patch-based visual CoT) and DeepEyes-7B (text-based visual CoT) by 9.5% and 2.7%, respectively (Table 1). In Figure 1, we plot bounding-box precision (IoU under the SFT setting with ground-truth coordinates) and final answer accuracy over the course of training. The results show that NV-CoT consistently improves **localization accuracy**, **final answer accuracy**, and **convergence speed**.

Our contributions are threefold:

- We propose NV-CoT, which expands the action space of MLLMs from discrete vocabulary tokens to a continuous Euclidean space, enabling the direct generation of numerical bounding box coordinates as actions.

- We develop Gaussian/Laplace coordinate policies with reparameterized sampling and analytic importance ratios, making continuous localization compatible with mainstream RL algorithms (*e.g.*, GRPO-style methods).
- We conduct experiments on three benchmarks against eight baseline models (including text-based and patch-based, as well as SFT-based and RL-based, “thinking with images” methods), demonstrating that NV-CoT significantly improves localization accuracy, final answer accuracy, and convergence speed.

2. Related Work

Multimodal large language models. By integrating language modeling capabilities with visual understanding, MLLMs enable complex vision-language tasks. Representative early models such as BLIP-2 (Li et al., 2023b) and LLaVA (Liu et al., 2023; 2024a) align vision and language by projecting image into the latent space of a frozen LLM via a query transformer or a lightweight projector. Subsequent strong open-source models, including the LLaVA family (Liu et al., 2024b; Guo et al., 2024; Zhang et al., 2025b; Lin et al., 2024; Li et al., 2023a; 2025a), Qwen-VL (Bai et al., 2023; Wang et al., 2024; Bai et al., 2025), and InternVL (Chen et al., 2024; Lu et al., 2025), further improve visual resolution handling and scalability. However, despite their strong perception and alignment capabilities, these models generally lack explicit reasoning mechanisms such as visual Chain-of-Thought (CoT).

Thinking with Images (visual CoT). Incorporating CoT reasoning to enhance visual understanding has been actively explored in recent MLLMs (Wang et al., 2025a; Zhang et al., 2025c). Early text-based approaches (Liu et al., 2025; Bai et al., 2025; Zhu et al., 2025) serialize localized image regions as bounding-box coordinates in text, and subsequently invoke cropping tools to extract the corresponding visual patches. While effective, this paradigm suffers from modality mismatch and semantic fragmentation. More recent patch-based methods (Li et al., 2026; Su et al., 2025a; Huang et al., 2025) instead operate directly on fine-grained visual patches, avoiding explicit textual serialization. However, these approaches are fundamentally constrained by the fixed spatial granularity of the vision backbone, limiting their flexibility in region selection and reasoning precision. In contrast, NV-CoT expands the MLLM action space from discrete vocabulary tokens to a continuous Euclidean space, enabling the model to directly predict numerical bounding-box coordinates as continuous actions. This design naturally bridges visual perception and reasoning, without relying on textual discretization or fixed patch partitions.

To incorporate CoT to MLLMs, existing methods adopt either supervised fine-tuning (Zhang et al., 2025a; Wang et al., 2025b; Chung et al., 2025; Shao et al., 2024a) or reinforce-

ment learning (Zhang et al., 2025c; Su et al., 2025b; Zheng et al., 2025; Zhao et al., 2025). Our approach is compatible with both paradigms, providing a unified framework for learning continuous visual actions.

3. Method

Given a query q and an image I_0 , a visual CoT MLLM π_θ performs region-grounded reasoning by selecting a region of interest and invoking a zoom-in function for fine-grained inspection. Existing visual-CoT methods localize regions by generating **text-form** box coordinates and then cropping the image for feedback. We instead cast localization as a continuous-action problem in Euclidean space: the MLLM directly outputs **numerical coordinates**. Our method proceeds in three steps. First, we expand the MLLM vocabulary with a continuous coordinate action space (Section 3.1), enabling numerical box generation. Second, we instantiate NV-CoT for SFT with coordinate regression when box supervision is available (Section 3.2). Third, we extend NV-CoT to GRPO by introducing a stochastic Gaussian policy with closed-form importance ratios and KL regularization (Section 3.3). Finally, we provide a Laplace-policy variant as a drop-in replacement, motivated by the empirical preference of ℓ_1 -type losses for localization (Section 3.4).

3.1. Expanded Actions for Continuous Coordinates

To enable numerical coordinate prediction, we augment the standard LLM output head over the vocabulary \mathcal{V} with a continuous action space $\mathcal{A} = \mathbb{R}^4 \times \mathbb{R}_+$: four coordinate heads parameterized by $W = [\mathbf{w}_{x_1}, \mathbf{w}_{y_1}, \mathbf{w}_{x_2}, \mathbf{w}_{y_2}]^\top \in \mathbb{R}^{4 \times D}$ to predict the Gaussian mean, and a fifth head $\mathbf{w}_\sigma \in \mathbb{R}^D$ to predict a shared standard deviation, yielding a Gaussian policy for continuous localization. Let $\mathbf{h} \in \mathbb{R}^D$ denote the final hidden representation before the coordinate decoding step. We obtain the mean as

$$\boldsymbol{\mu} = [x_1, y_1, x_2, y_2]^\top = W\mathbf{h}, \quad (1)$$

and predict a shared standard deviation as

$$\sigma = \max(\mathbf{w}_\sigma^\top \mathbf{h}, \varepsilon), \quad (2)$$

where $\varepsilon > 0$ is a small positive offset to ensure $\sigma > 0$. This forms a Gaussian policy $\mathcal{N}(\boldsymbol{\mu}, \sigma^2 I)$. Accordingly, we augment the parameter set as $\theta \leftarrow \theta \cup \{W, \mathbf{w}_\sigma\}$.

The introduction of σ is crucial: while deterministic coordinate suffices for SFT, GRPO-style RL requires stochastic policies to enable sampling and exploration. Note that our modification to the MLLM is minimal, as we only introduce five lightweight linear heads, in contrast to patch-based visual CoT methods that require more architectural changes.

3.2. NV-CoT for Supervised Fine-Tuning

We begin by applying our NV-CoT to supervised fine-tuning, where intermediate bounding-box coordinates in the reasoning process are available (Chung et al., 2025; Shao et al., 2024a). Let $\mathbf{b}^* = [x_1^*, y_1^*, x_2^*, y_2^*]^\top$ denote the ground-truth bounding box for a zoom-in step. During SFT, we supervise the coordinate outputs in \mathcal{A} using an ℓ_2^2 regression loss, while optimizing the discrete token outputs in the original LLM head \mathcal{V} with the standard cross-entropy loss.

$$\mathcal{L}_{\text{SFT}}(\theta) = \sum_{t \in \mathcal{T}_{\mathcal{V}}} \left(-\log \pi_{\theta}(o_t \mid o_{<t}, q, I_0) \right) + \lambda \sum_{t \in \mathcal{T}_{\mathcal{A}}} \|\boldsymbol{\mu}_t - \mathbf{b}_t^*\|_2^2, \quad (3)$$

where $\mathcal{T}_{\mathcal{V}} = \{t : o_t \in \mathcal{V}\}$ and $\mathcal{T}_{\mathcal{A}} = \{t : o_t \in \mathcal{A}\}$ denote textual token and coordinate-action positions, respectively; $\lambda > 0$ is a hyperparameter; σ is not supervised in SFT and is only used for RL.

3.3. NV-CoT for Reinforcement Learning

Bounding-box annotations for SFT are costly and often unavailable at scale. As a result, visual-CoT models are commonly trained with RL (GRPO Shao et al. (2024b)) using task-level feedback (e.g., final answer) as the reward signal, without requiring box-level supervision. Extending NV-CoT from SFT to this RL setting, however, is non-trivial: RL needs stochastic sampling and well-defined importance ratios, whereas standard LLM policies are token-level categorical distributions that do not accommodate continuous coordinate actions. To this end, we formulate continuous region localization as a Gaussian policy over the action space \mathcal{A} .

Rollouts. GRPO samples a group of G trajectories per prompt. With our Gaussian policy, we draw coordinate actions independently as $\mathbf{b}^{(i)} \sim \mathcal{N}(\boldsymbol{\mu}, \sigma^2 I)$, $i = 1, \dots, G$, implemented via the reparameterization trick,

$$\mathbf{b}^{(i)} = \boldsymbol{\mu} + \sigma \boldsymbol{\epsilon}^{(i)}, \quad \boldsymbol{\epsilon}^{(i)} \sim \mathcal{N}(\mathbf{0}, I), \quad (4)$$

which enables low-variance gradient estimation. We then use $\mathbf{b}^{(i)}$ to crop into the image for the i -th trajectory.

Importance ratio. GRPO optimizes the policy via an importance ratio between the current policy π_{θ} and a reference policy $\pi_{\theta_{\text{old}}}$. For each output $o_t^{(i)}$, the ratio is defined as

$$r_t^{(i)}(\theta) = \frac{\pi_{\theta}(o_t^{(i)} \mid q, I_0, o_{<t}^{(i)})}{\pi_{\theta_{\text{old}}}(o_t^{(i)} \mid q, I_0, o_{<t}^{(i)})}. \quad (5)$$

When $o_t^{(i)} \in \mathcal{V}$ is a text token, $r_t^{(i)}(\theta)$ reduces to the standard likelihood ratio of categorical policies used in GRPO.

When $o_t^{(i)} \in \mathcal{A}$ corresponds to a continuous coordinate action $\mathbf{b}_t^{(i)}$, we compute the ratio using Gaussian likelihoods:

$$r_t^{(i)}(\theta) = \frac{\mathcal{N}(\mathbf{b}_t^{(i)} \mid \boldsymbol{\mu}_{\theta}, \sigma_{\theta}^2 I)}{\mathcal{N}(\mathbf{b}_t^{(i)} \mid \boldsymbol{\mu}_{\theta_{\text{old}}}, \sigma_{\theta_{\text{old}}}^2 I)}. \quad (6)$$

Recall that the multivariate Gaussian density is given by

$$\mathcal{N}(\mathbf{b} \mid \boldsymbol{\mu}, \sigma^2 I) = \frac{1}{(2\pi\sigma^2)^{d/2}} \exp\left(-\frac{\|\mathbf{b} - \boldsymbol{\mu}\|_2^2}{2\sigma^2}\right), \quad (7)$$

where $d = 4$ in our case. Substituting this form into the ratio, we obtain the importance ratio that depends on the squared Mahalanobis distances:

$$r_t^{(i)}(\theta) = \frac{\sigma_{\theta_{\text{old}}}^4}{\sigma_{\theta}^4} \exp\left(-\frac{\|\mathbf{b}_t^{(i)} - \boldsymbol{\mu}_{\theta}\|_2^2}{2\sigma_{\theta}^2} + \frac{\|\mathbf{b}_t^{(i)} - \boldsymbol{\mu}_{\theta_{\text{old}}}\|_2^2}{2\sigma_{\theta_{\text{old}}}^2}\right). \quad (8)$$

KL penalty. Thanks to the closed-form KL divergence of Gaussian distributions, this penalty is analytically tractable for continuous actions \mathcal{A} :

$$\text{KL}(\pi_{\theta} \parallel \pi_{\text{ref}}) = \frac{\|\boldsymbol{\mu}_{\theta} - \boldsymbol{\mu}_{\text{ref}}\|_2^2}{2\sigma_{\text{ref}}^2} + 2\left(\frac{\sigma_{\theta}^2}{\sigma_{\text{ref}}^2} - \log \sigma_{\theta}^2\right) + C, \quad (9)$$

where C is a constant. However, σ_{ref} is unknown since σ is not supervised in SFT. Therefore, we drop the variance-related term and only constrain the mean: $\text{KL}_{\boldsymbol{\mu}}(\pi_{\theta} \parallel \pi_{\text{ref}}) = \|\boldsymbol{\mu}_{\theta} - \boldsymbol{\mu}_{\text{ref}}\|_2^2$. If SFT stage is unavailable (and thus no reference mean $\boldsymbol{\mu}_{\text{ref}}$ can be obtained), we omit this KL regularization term. For textual token outputs in \mathcal{V} , we retain the standard token-level KL divergence.

Reward. Following DeepEyes (Zheng et al., 2025), we adopt an outcome-driven reward that combines answer correctness, format validity, and a conditional zoom-in use bonus. Formally, for a trajectory $o^{(i)}$, the total reward is

$$R(o^{(i)}) = R_{\text{acc}}(o^{(i)}) + R_{\text{fmt}}(o^{(i)}) + R_{\text{zoom}}(o^{(i)}), \quad (10)$$

where the zoom-in bonus is activated only when the trajectory is correct and invokes the visual grounding action at least once, encouraging region of interest identification.

Optimization. Finally, given a question q and an input image I_0 , we sample a group of G trajectories $\{o^{(1)}, \dots, o^{(G)}\}$ from $\pi_{\theta_{\text{old}}}$, each associated with intermediate bounding boxes $\{\mathbf{b}^{(1)}, \dots, \mathbf{b}^{(G)}\}$ (via Eq. (4)). We compute trajectory-level rewards $\mathbf{R} = \{R(o^{(1)}), \dots, R(o^{(G)})\}$ using Eq. (10) and use the normalized advantage for all steps in the i -th trajectory: $A_t^{(i)} = \frac{R(o^{(i)}) - \text{mean}(\mathbf{R})}{\text{std}(\mathbf{R})}$. Given the importance ratio $r_t^{(i)}(\theta)$ and the KL term $\text{KL}(\pi_{\theta} \parallel \pi_{\text{ref}})$

defined above, we optimize the following objective:

$$\mathcal{L}_{\text{GRPO}}(\theta) = \mathbb{E}_{q, I_0, \{o^{(i)}\}_{i=1}^G \sim \pi_{\theta_{\text{old}}}} \left[\frac{1}{GT} \sum_{i=1}^G \sum_{t=1}^T \min \left(r_t^{(i)}(\theta) A_t^{(i)}, \text{clip}(r_t^{(i)}(\theta), 1 - \varepsilon, 1 + \varepsilon) A_t^{(i)} \right) - \beta \text{KL}(\pi_{\theta} \parallel \pi_{\text{ref}}) \right], \quad (11)$$

where $\varepsilon > 0$ is the clipping range.

Inference. During inference, we disable stochasticity and directly use the coordinate mean $\boldsymbol{\mu}$ to crop the image.

3.4. Extending NV-CoT with Laplace Policy

In prediction tasks such as keypoint localization and bounding-box regression, it is well known that ℓ_1 loss often outperforms ℓ_2^2 loss due to its robustness to outliers and sharper error profiles (Girshick, 2015; Sun et al., 2018). From a probabilistic perspective, this corresponds to modeling prediction errors with a Laplace distribution rather than a Gaussian distribution. Motivated by this observation, we further extend NV-CoT by replacing the Gaussian policy with a Laplace policy for continuous localization.

Laplace policy. Specifically, we model the coordinate action as $\mathbf{b} \sim \text{Laplace}(\boldsymbol{\mu}, \alpha)$, whose probability density function is

$$p(\mathbf{b} \mid \boldsymbol{\mu}, \alpha) = \frac{1}{(2\alpha)^4} \exp\left(-\frac{\|\mathbf{b} - \boldsymbol{\mu}\|_1}{\alpha}\right), \quad (12)$$

where $\boldsymbol{\mu} \in \mathbb{R}^4$ denotes the predicted coordinate mean and $b > 0$ is a shared scale parameter. Equivalently, this corresponds to assuming independent dimensions, under which the Laplace likelihood factorizes across coordinates.

SFT objective. Under the Laplace assumption, maximizing the log-likelihood of ground-truth coordinates is equivalent to minimizing an ℓ_1 loss, since $-\log p(\mathbf{b}^* \mid \boldsymbol{\mu}, \alpha) = \frac{1}{\alpha} \|\boldsymbol{\mu} - \mathbf{b}^*\|_1 + \text{const}$. Thus, in the SFT stage, we replace the ℓ_2^2 loss Eq. (3) with

$$\mathcal{L}_{\text{SFT}}^{\text{Lap}}(\theta) = \sum_{t \in \mathcal{Y}_A} \|\boldsymbol{\mu}_t - \mathbf{b}_t^*\|_1, \quad (13)$$

which encourages sharper and more robust localization.

RL with Laplace policy. Analogous to the Gaussian case, we parameterize the Laplace policy with a location parameter $\boldsymbol{\mu}$ and a scale parameter α , and employ reparameterized sampling to enable low-variance gradient estimation. Specifically, a coordinate action is sampled as

$$\mathbf{b} = \boldsymbol{\mu} + \alpha \mathbf{s} \odot \boldsymbol{\epsilon}, \quad \mathbf{s} \sim \text{Rademacher}(\pm 1), \quad \boldsymbol{\epsilon} \sim \text{Exp}(\mathbf{1}), \quad (14)$$

where \odot denotes element-wise multiplication. Here, \mathbf{s} is a random sign vector with i.i.d. entries in $\{\pm 1\}$, and $\boldsymbol{\epsilon}$ has i.i.d. unit-rate exponential entries. For a sampled action $\mathbf{b}_t^{(i)}$, the corresponding importance ratio used in GRPO is

$$r_t^{(i)}(\theta) = \frac{\alpha_{\theta_{\text{old}}}^4}{\alpha_{\theta}^4} \exp\left(-\frac{\|\mathbf{b}_t^{(i)} - \boldsymbol{\mu}_{\theta}\|_1}{\alpha_{\theta}} + \frac{\|\mathbf{b}_t^{(i)} - \boldsymbol{\mu}_{\theta_{\text{old}}}\|_1}{\alpha_{\theta_{\text{old}}}}\right), \quad (15)$$

which can be computed analytically. The closed-form KL penalty can be derived analogously, and the overall GRPO procedure follows the same pipeline as in the Gaussian-policy case.

4. Experiments

4.1. Setup

Baselines. To evaluate the effectiveness of NV-CoT, we compare against eight state-of-the-art MLLM baselines, grouped into the following three categories:

- *Open-source MLLMs.* This category includes Qwen2.5-VL- $\{7\text{B}, 32\text{B}\}$ (Bai et al., 2025) and LLaVA-OneVision (Li et al., 2025a).
- *Supervised fine-tuning based visual CoT.* We compare against Vis-CoT-7B (Shao et al., 2024a), which leverages annotated intermediate bounding boxes for supervision.
- *Reinforcement learning based visual CoT.* These methods do not assume access to annotated bounding-box. We further divide them into two subgroups: (I) *Text-based visual CoT.* UV-CoT-7B (Zhao et al., 2025) uses an LLM-as-a-judge to rank trajectory pairs and optimizes a DPO-style objective (Rafailov et al., 2023). DeepEyes-7B (Zheng et al., 2025) applies GRPO-style RL with final answer accuracy as the reward. (II) *Patch-based visual CoT.* PaDT (Su et al., 2025a) generates discrete patch indices/tokens for fine-grained reasoning, while LVR (Li et al., 2026) performs reasoning over latent visual patches.

Our NV-CoT is applicable to both SFT and RL settings. In this work, we build the SFT-based model upon Vis-CoT (Shao et al., 2024a) and the RL-based model upon DeepEyes (Zheng et al., 2025).

Datasets. For fair comparison, we use the *same training data* as the corresponding backbones (e.g., DeepEyes-7B and Vis-CoT-7B). For evaluation, we adopt V^* Bench (Wu & Xie, 2024), HR-Bench 4K (Wang et al., 2025c), and HR-Bench 8K (Wang et al., 2025c), which assess MLLMs’ ability in fine-grained visual detail search and relative spatial reasoning across image resolutions ranging from 2K to 8K. Specifically, V^* Bench measures attribute reasoning (Attr) and spatial reasoning (Spatial); HR-Bench focuses on fine-grained spatial perception (FSP) and fine-grained comparison perception (FCP), as well as overall performance.

Table 1. Overall comparison of different models on three benchmarks. The **best** results are in bold. Our NV-CoT consistently improves performance under both SFT and RL settings. We use NV-CoT (SFT) with an ℓ_1 loss and NV-CoT (RL) with a Laplace policy. **DeepEyes-7B[†]** and **NV-CoT[†]** denote results under multi-step tool use (multiple zoom-in calls). For a fair comparison, all other visual CoT methods are evaluated with a single zoom-in call, since some baselines do not support multiple tool invocations.

Model	V* Bench			HR Bench 4K			HR Bench 8K		
	Attr	Spatial	Overall	FSP	FCP	Overall	FSP	FCP	Overall
LLaVA-OneVision-7B	75.7	75.0	75.4	71.7	53.3	62.5	69.1	52.1	60.6
Qwen2.5-VL-7B	73.9	67.1	71.2	84.7	52.9	68.8	78.7	51.8	65.3
Qwen2.5-VL-32B	87.8	88.1	87.9	89.4	58.3	73.9	83.6	56.9	70.3
PaDT-7B	75.7	73.6	74.9	86.0	54.8	70.4	79.0	53.8	66.4
LVR-7B	84.4	76.3	81.2	88.3	56.8	72.5	82.5	54.5	68.5
UV-CoT-7B	82.6	76.3	80.1	79.8	54.5	67.1	76.8	54.3	65.5
Vis-CoT-7B	80.9	75.0	78.5	79.0	54.3	66.6	75.5	53.0	64.3
+ NV-CoT (SFT)	84.3	78.9	82.2	82.0	55.3	68.6	77.3	54.5	65.9
Δ	+3.5	+3.9	+3.7	+3.0	+1.0	+2.0	+1.8	+1.5	+1.6
DeepEyes-7B	87.8	84.2	86.4	89.3	57.8	73.5	84.3	56.5	70.4
+ NV-CoT (RL)	90.4	86.8	89.0	91.0	58.5	74.8	85.8	58.3	72.0
Δ	+2.6	+2.6	+2.6	+1.7	+0.7	+1.3	+1.5	+1.8	+1.6
DeepEyes-7B [†]	91.3	88.2	90.1	91.3	59.0	75.2	86.8	58.5	72.7
+ NV-CoT [†] (RL)	93.0	89.5	91.6	91.8	60.3	76.0	87.5	60.0	73.8
Δ	+1.7	+1.3	+1.5	+0.5	+1.3	+1.1	+0.7	+1.5	+1.2

Evaluation protocols. For a fair comparison under identical inference scaling, we evaluate all models with a single tool call (zoom-in) per query, since some baselines (e.g., Vis-CoT (Shao et al., 2024a) and UV-CoT (Zhao et al., 2025)) do not support iterative tool invocations. For methods that do support multiple tool calls (e.g., DeepEyes (Zheng et al., 2025) and our NV-CoT (RL)), we additionally report results under multiple tool use.

Implementation details. To ensure a fair comparison, we keep the training configurations identical to those of the backbone methods (DeepEyes-7B (Zheng et al., 2025) and Vis-CoT-7B (Shao et al., 2024a)), and only replace text-form coordinate prediction with our continuous action formulation. Specifically, for SFT, we fine-tune LLaVA for one epoch with a batch size of 128. We use the Adam optimizer with zero weight decay, a learning rate of 2×10^{-5} , and a cosine learning-rate scheduler. λ in Eq. (3) is set to 0.3. For RL, we train the RL-based model on top of Qwen2.5-VL-7B using GRPO for 80 iterations on 32 A100 GPUs. We set the batch size to 256 and the GRPO group size to $G = 16$. The KL coefficient is set to $\beta = 0$.

4.2. Main Results

The overall performance comparisons are reported in Table 1, leading to the following key observations:

(1) Our NV-CoT consistently outperforms the backbone models across all benchmarks under both SFT and RL. Specifically, under SFT, NV-CoT improves over Vis-CoT-7B by +3.4% overall on V* Bench, +2.0% on HR-

Bench 4K, and +1.5% on HR-Bench 8K. Under RL, NV-CoT achieves further gains over DeepEyes-7B, with overall improvements of +2.7%, +1.3%, and +1.8% on the three benchmarks, respectively. These results suggest that replacing text-based bounding-box prediction with our numerical one benefits both SFT and RL training paradigms.

(2) We observe a clear paradigm advantage of zoom-in visual CoT over patch-based reasoning. The backbone DeepEyes-7B and our NV-CoT (RL) consistently outperform patch-based baselines such as PaDT-7B and LVR-7B across all benchmarks, suggesting that region selection via zoom-in is more effective than reasoning over fixed-granularity patches.

(3) Methods that perform thinking with images substantially outperform basic MLLMs such as LLaVA-OneVision-7B and Qwen2.5-VL-7B. Notably, despite being built on a 7B backbone, NV-CoT achieves performance that surpasses Qwen2.5-VL-32B across all benchmarks. This highlights the importance of region-grounded visual reasoning in improving multimodal understanding.

(4) Allowing multiple zoom-in tool calls further improves “thinking with images” performance, indicating that iterative region selection and refinement is beneficial for fine-grained visual reasoning. Notably, DeepEyes-7B[†] achieves consistently higher scores than its single-call counterpart across all benchmarks. Building on this stronger multi-step setting, NV-CoT[†] further boosts performance by replacing textified coordinates with continuous coordinate actions, enabling more precise region localization.

Table 2. Ablation on coordinate policy (Gaussian (ℓ_2^2) vs. Laplace (ℓ_1)) and uncertainty parameterization (shared σ/α vs. per-coordinate σ/α). Non-shared σ/α : per-coordinate scale (standard deviation) predicted by four heads. Laplace policy consistently performs better than Gaussian policy, while using a shared versus per-coordinate σ/α yields comparable results.

Model		V^* Bench			HR Bench 4K			HR Bench 8K		
		Attr	Spatial	Overall	FSP	FCP	Overall	FSP	FCP	Overall
SFT	ℓ_2^2 loss	83.5	76.3	80.6	81.5	53.5	67.5	76.0	54.3	65.1
	ℓ_1 loss	84.3	78.9	82.2	82.0	55.3	68.6	77.3	54.5	65.9
RL	Gaussian policy	88.7	85.5	87.4	90.3	58.3	74.3	85.0	58.0	71.5
	+ Independent σ	87.8	86.8	87.4	90.0	58.3	74.1	85.5	57.8	71.6
	Laplace policy	90.4	86.8	89.0	91.0	58.5	74.8	85.8	58.3	72.0
	+ Independent α	89.6	86.8	88.5	90.8	58.8	74.8	86.0	58.3	72.1

Table 3. Bounding-box IoU on the Vis-CoT-363K dataset. NV-CoT substantially improves localization precision over Vis-CoT, with the ℓ_1 loss outperforming the ℓ_2^2 loss.

	Vis-CoT	NV-CoT (ℓ_2^2)	NV-CoT (ℓ_1)
Bbox IoU	47.3	57.4	59.5

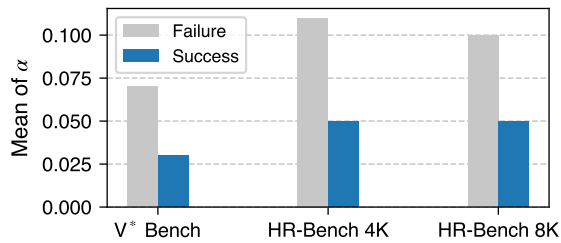


Figure 3. Behavior of α . Successful trajectories exhibit smaller α than failed ones, reflecting higher confidence.

4.3. Ablation Studies

This section presents ablation studies on (i) the coordinate policy family (Gaussian/ ℓ_2^2 vs. Laplace/ ℓ_1), and (ii) the uncertainty parameterization, comparing a shared scalar dispersion parameter (Gaussian σ or Laplace α) against independent per-coordinate parameters (Gaussian $\sigma \in \mathbb{R}_+^4$ or Laplace $\alpha \in \mathbb{R}_+^4$), as summarized in Table 2 and Table 3.

Regression loss and policy distribution. We jointly analyze the choice of regression loss in SFT and policy distribution in RL, as both stages reflect continuous modeling of coordinates. In the SFT stage, the ℓ_1 loss consistently outperforms the ℓ_2^2 loss across all benchmarks, improving overall accuracy on V^* Bench by +1.5% and yielding consistent gains on HR-Bench 4K (+1.1%) and 8K (+0.6%). These trends carry over to RL: the Laplace policy consistently outperforms the Gaussian policy on all benchmarks. This is consistent with prior observations in bounding-box and keypoint regression that ℓ_1 -type objectives are more robust for localization.

Under SFT, we further measure bounding-box IoU on the

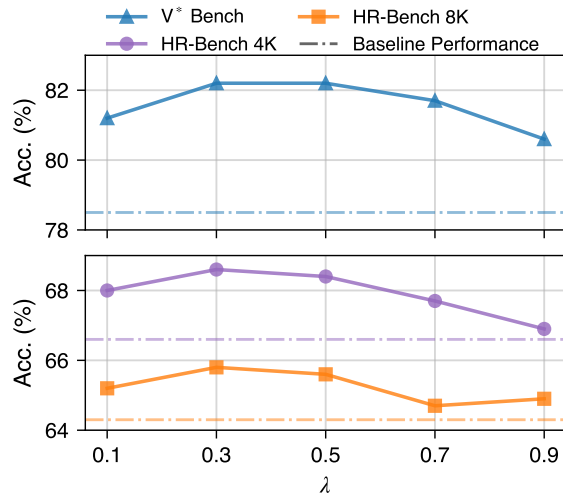


Figure 4. Effect of λ . Performance peaks at $\lambda = 0.3$ and NV-CoT consistently outperforms the baseline across all values.

Vis-CoT-363K validation set. As shown in Table 3, NV-CoT significantly improves localization accuracy over Vis-CoT, with the ℓ_1 loss achieving the best IoU.

Shared vs. independent σ/α parameterization. We further investigate whether the dispersion parameter should be shared across coordinates or predicted independently. Taking the Gaussian policy as an example, we extend the model with four additional heads $\Sigma = [\mathbf{w}_{\sigma, x_1}, \mathbf{w}_{\sigma, y_1}, \mathbf{w}_{\sigma, x_2}, \mathbf{w}_{\sigma, y_2}]^\top$ to predict per-coordinate standard deviations. Specifically, the independent standard deviations are given by

$$\sigma = [\sigma_1, \sigma_2, \sigma_3, \sigma_4]^\top = \max(\Sigma \mathbf{h}, \varepsilon), \quad (16)$$

which generalizes the shared-variance formulation in Eq. (2). Now, the importance ratio changes to:

$$r(\theta) = \prod_{j=1}^4 \frac{\sigma_{\theta_{\text{old}, j}}}{\sigma_{\theta, j}} \exp\left(-\frac{(b_j - \mu_{\theta, j})^2}{2\sigma_{\theta, j}^2} + \frac{(b_j - \mu_{\theta_{\text{old}, j}})^2}{2\sigma_{\theta_{\text{old}, j}}^2}\right). \quad (17)$$

The Laplace policy follows an analogous procedure. As shown in Table 2, the performance gap between shared

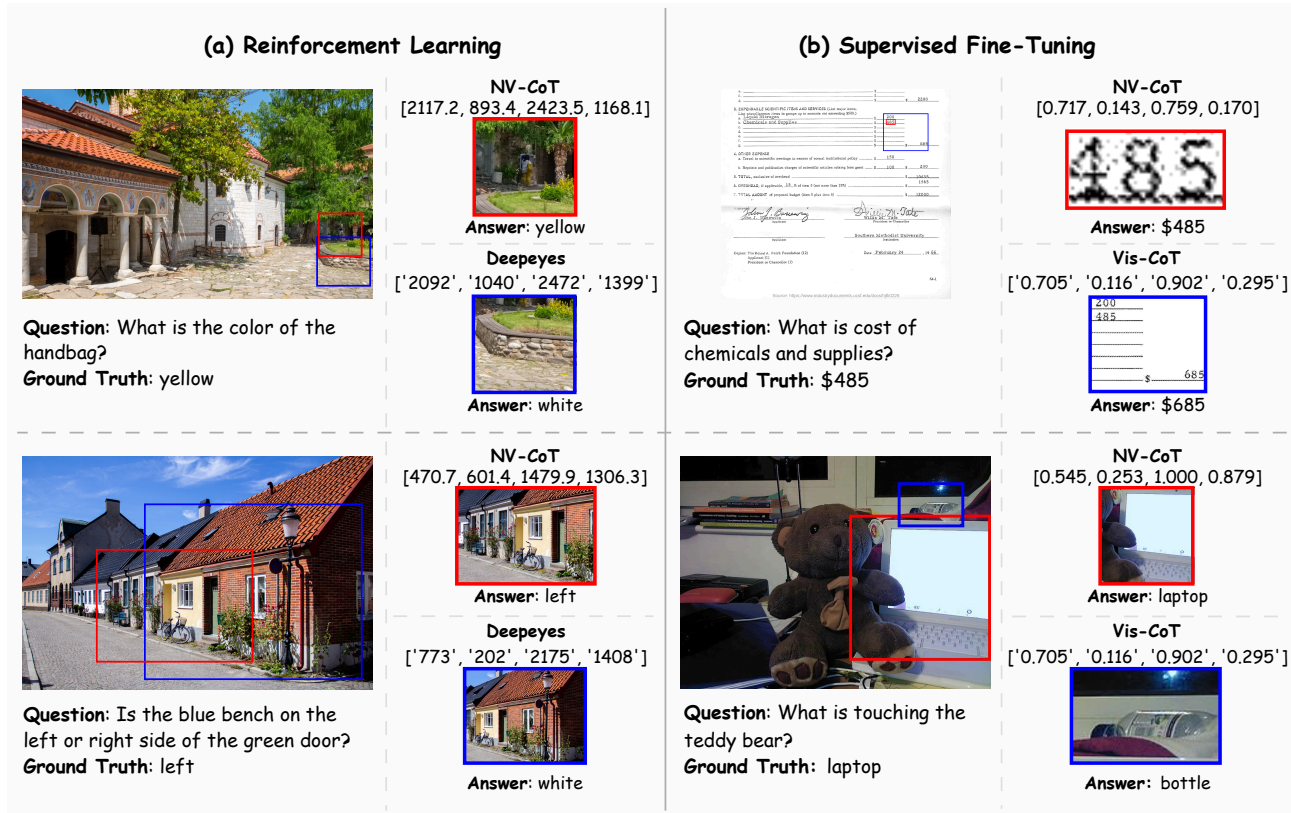


Figure 5. Visualization of bounding boxes. NV-CoT produces more accurate bounding boxes (shown in red) compared to the backbone model (shown in blue), demonstrating improved localization capability.

and independent parameterizations is marginal across all benchmarks. Given the comparable results, we adopt a shared σ/α in our final model for simplicity and efficiency.

4.4. Other Analyses

Behavior analysis of α . In Figure 3, we analyze the behavior of the Laplace scale parameter α by comparing its average values across success and failure cases. Results across different image resolutions are normalized. Successful trajectories consistently exhibit smaller α than failed ones. This observation indicates that accurate localization is associated with lower predictive uncertainty, leading the policy to produce more concentrated bounding-box samples.

Effect of λ . In Figure 4, we study the effect of λ in Eq. (3) by varying it from 0.1 to 0.9 and reporting overall accuracy on three benchmarks. NV-CoT achieves the best performance at $\lambda = 0.3$, while maintaining relatively stable accuracy across a wide range of values. Notably, across all λ settings, NV-CoT consistently outperforms the text-based baselines by a clear margin, indicating that the performance gains are robust and not sensitive to the choice of λ .

Visualization. In Figure 5, we present qualitative comparisons of bounding-box localization between NV-CoT and

the backbone model. The backbone model (blue) often produces coarse or loosely aligned bounding boxes that either cover excessive background regions or partially miss the target objects. In contrast, NV-CoT (red) consistently generates tighter and more accurate bounding boxes that better align with the true object extents. The visualizations demonstrate that modeling bounding-box coordinates as continuous actions enables NV-CoT to capture spatial structure more effectively, resulting in improved localization quality and reduced ambiguity in region grounding.

5. Conclusion

We present NV-CoT, a plug-and-play framework that enables MLLMs to directly generate continuous bounding-box coordinates instead of textual tokens. By formulating localization as a continuous-action problem with Gaussian/Laplace policies, NV-CoT supports both supervised fine-tuning and reinforcement learning. NV-CoT mitigates the modality mismatch and semantic fragmentation of text-based visual CoT, while avoiding the fixed-granularity limitation of patch-based designs, with only minimal architectural modifications. Experiments on three benchmarks demonstrate consistent improvements in localization precision, final answer accuracy and training efficiency.

Impact Statements

This paper presents work whose primary goal is to advance the capabilities of multimodal large language models in visual reasoning, particularly through more accurate and efficient region grounding. By enabling models to reason over images using continuous numerical representations, our approach improves localization precision and training efficiency, which may benefit a wide range of downstream applications such as visual question answering and optical character recognition. At the same time, improved visual localization and reasoning capabilities could be applied in sensitive domains. However, our work does not introduce new data sources, deployable systems, or application-specific pipelines, and it relies on standard benchmark datasets commonly used in the research community. As such, we do not believe that this work introduces novel ethical risks beyond those already well recognized in the field of MLLMs.

References

- Bai, J., Bai, S., Chu, Y., Cui, Z., Dang, K., Deng, X., Fan, Y., Ge, W., Han, Y., Huang, F., et al. Qwen technical report. *arXiv preprint arXiv:2309.16609*, 2023.
- Bai, S., Chen, K., Liu, X., Wang, J., Ge, W., Song, S., Dang, K., Wang, P., Wang, S., Tang, J., et al. Qwen2. 5-vl technical report. *arXiv preprint arXiv:2502.13923*, 2025.
- Chen, Z., Wu, J., Wang, W., Su, W., Chen, G., Xing, S., Zhong, M., Zhang, Q., Zhu, X., Lu, L., et al. Internvl: Scaling up vision foundation models and aligning for generic visual-linguistic tasks. In *CVPR*, 2024.
- Chung, J., Kim, J., Kim, S., Lee, J., Kim, M. S., and Yu, Y. Don't look only once: Towards multimodal interactive reasoning with selective visual revisitation. *arXiv preprint arXiv:2505.18842*, 2025.
- Girshick, R. Fast r-cnn. In *ICCV*, 2015.
- Guo, Z., Xu, R., Yao, Y., Cui, J., Ni, Z., Ge, C., Chua, T.-S., Liu, Z., and Huang, G. Llava-uhd: an lmm perceiving any aspect ratio and high-resolution images. In *ECCV*, 2024.
- Huang, Z., Chen, K., He, J., Bai, X., Karatzas, D., Lu, S., and Jawahar, C. Icdar2019 competition on scanned receipt ocr and information extraction. In *2019 International Conference on Document Analysis and Recognition (ICDAR)*, 2019.
- Huang, Z., Ji, Y., Rajan, A. S., Cai, Z., Xiao, W., Wang, H., Hu, J., and Lee, Y. J. Visualtoolagent (vista): A reinforcement learning framework for visual tool selection. *arXiv preprint arXiv:2505.20289*, 2025.
- Hudson, D. A. and Manning, C. D. Gqa: A new dataset for real-world visual reasoning and compositional question answering. In *CVPR*, 2019.
- Li, B., Zhang, Y., Guo, D., Zhang, R., Li, F., Zhang, H., Zhang, K., Zhang, P., Li, Y., Liu, Z., et al. Llava-onevision: Easy visual task transfer. *TMLR*, 2025a.
- Li, B., Sun, X., Liu, J., Wang, Z., Wu, J., Yu, X., Chen, H., Barsoum, E., Chen, M., and Liu, Z. Latent visual reasoning. In *arXiv preprint arXiv:2509.24251*, 2026.
- Li, C., Wong, C., Zhang, S., Usuyama, N., Liu, H., Yang, J., Naumann, T., Poon, H., and Gao, J. Llava-med: Training a large language-and-vision assistant for biomedicine in one day. In *NeurIPS*, 2023a.
- Li, C., Wu, W., Zhang, H., Xia, Y., Mao, S., Dong, L., Vulić, I., and Wei, F. Imagine while reasoning in space: Multimodal visualization-of-thought. In *ICML*, 2025b.
- Li, J., Li, D., Savarese, S., and Hoi, S. Blip-2: Bootstrapping language-image pre-training with frozen image encoders and large language models. In *ICML*, 2023b.
- Li, L., Wang, Y., Xu, R., Wang, P., Feng, X., Kong, L., and Liu, Q. Multimodal arxiv: A dataset for improving scientific comprehension of large vision-language models. *arXiv preprint arXiv:2403.00231*, 2024.
- Lin, B., Ye, Y., Zhu, B., Cui, J., Ning, M., Jin, P., and Yuan, L. Video-llava: Learning united visual representation by alignment before projection. In *EMNLP*, 2024.
- Liu, H., Li, C., Wu, Q., and Lee, Y. J. Visual instruction tuning. In *NeurIPS*, 2023.
- Liu, H., Li, C., Li, Y., and Lee, Y. J. Improved baselines with visual instruction tuning. In *CVPR*, 2024a.
- Liu, S., Cheng, H., Liu, H., Zhang, H., Li, F., Ren, T., Zou, X., Yang, J., Su, H., Zhu, J., et al. Llava-plus: Learning to use tools for creating multimodal agents. In *ECCV*, 2024b.
- Liu, Y., Qu, T., Zhong, Z., Peng, B., Liu, S., Yu, B., and Jia, J. Visionreasoner: Unified visual perception and reasoning via reinforcement learning. *arXiv preprint arXiv:2505.12081*, 2025.
- Lu, D., Sun, Y., Zhang, Z., Huang, L., Zeng, J., Shu, M., and Cao, H. Internvl-x: Advancing and accelerating internvl series with efficient visual token compression. *arXiv preprint arXiv:2503.21307*, 2025.
- Mathew, M., Karatzas, D., and Jawahar, C. Docvqa: A dataset for vqa on document images. In *Proceedings of the IEEE/CVF winter conference on applications of computer vision*, pp. 2200–2209, 2021.

- Mathew, M., Bagal, V., Tito, R., Karatzas, D., Valveny, E., and Jawahar, C. Infographicvqa. In *Proceedings of the IEEE/CVF Winter Conference on Applications of Computer Vision*, pp. 1697–1706, 2022.
- Plummer, B. A., Wang, L., Cervantes, C. M., Caicedo, J. C., Hockenmaier, J., and Lazebnik, S. Flickr30k entities: Collecting region-to-phrase correspondences for richer image-to-sentence models. In *ICCV*, 2015.
- Rafailov, R., Sharma, A., Mitchell, E., Manning, C. D., Ermon, S., and Finn, C. Direct preference optimization: Your language model is secretly a reward model. In *NeurIPS*, 2023.
- Shao, H., Qian, S., Xiao, H., Song, G., Zong, Z., Wang, L., Liu, Y., and Li, H. Visual cot: Advancing multi-modal language models with a comprehensive dataset and benchmark for chain-of-thought reasoning. In *NeurIPS*, 2024a.
- Shao, Z., Wang, P., Zhu, Q., Xu, R., Song, J., Bi, X., Zhang, H., Zhang, M., Li, Y. K., Wu, Y., and Guo, D. Deepseekmath: Pushing the limits of mathematical reasoning in open language models, 2024b. URL <https://arxiv.org/abs/2402.03300>.
- Singh, A., Natarajan, V., Shah, M., Jiang, Y., Chen, X., Batra, D., Parikh, D., and Rohrbach, M. Towards vqa models that can read. In *CVPR*, 2019.
- Su, Y., Zhang, H., Li, S., Liu, N., Liao, J., Pan, J., Liu, Y., Xing, X., Sun, C., Li, C., et al. Patch-as-decodable-token: Towards unified multi-modal vision tasks in mllms. *arXiv preprint arXiv:2510.01954*, 2025a.
- Su, Z., Li, L., Song, M., Hao, Y., Yang, Z., Zhang, J., Chen, G., Gu, J., Li, J., Qu, X., et al. Openthinking: Learning to think with images via visual tool reinforcement learning. *arXiv preprint arXiv:2505.08617*, 2025b.
- Sun, X., Xiao, B., Wei, F., Liang, S., and Wei, Y. Integral human pose regression. In *ECCV*, 2018.
- Van Landeghem, J., Tito, R., Borchmann, Ł., Pietruszka, M., Joziak, P., Powalski, R., Jurkiewicz, D., Coustaty, M., Anckaert, B., Valveny, E., et al. Document understanding dataset and evaluation (dude). In *ICCV*, 2023.
- Wang, H., Su, A., Ren, W., Lin, F., and Chen, W. Pixel reasoner: Incentivizing pixel-space reasoning with curiosity-driven reinforcement learning. In *NeurIPS*, 2025a.
- Wang, J., Kang, Z., Wang, H., Jiang, H., Li, J., Wu, B., Wang, Y., Ran, J., Liang, X., Feng, C., et al. Vgr: Visual grounded reasoning. *arXiv preprint arXiv:2506.11991*, 2025b.
- Wang, P., Bai, S., Tan, S., Wang, S., Fan, Z., Bai, J., Chen, K., Liu, X., Wang, J., Ge, W., et al. Qwen2-vl: Enhancing vision-language model’s perception of the world at any resolution. *arXiv preprint arXiv:2409.12191*, 2024.
- Wang, W., Ding, L., Zeng, M., Zhou, X., Shen, L., Luo, Y., Yu, W., and Tao, D. Divide, conquer and combine: A training-free framework for high-resolution image perception in multimodal large language models. In *AAAI*, 2025c.
- Wang, X., Yang, Z., Feng, C., Lu, H., Li, L., Lin, C.-C., Lin, K., Huang, F., and Wang, L. Sota with less: Mcts-guided sample selection for data-efficient visual reasoning self-improvement. *arXiv preprint arXiv:2504.07934*, 2025d.
- Wu, P. and Xie, S. V*: Guided visual search as a core mechanism in multimodal llms. In *CVPR*, 2024.
- Zhang, G., Zhong, T., Xia, Y., Liu, M., Yu, Z., Li, H., He, W., Shu, F., She, D., Wang, Y., et al. Cmmcot: Enhancing complex multi-image comprehension via multi-modal chain-of-thought and memory augmentation. *arXiv preprint arXiv:2503.05255*, 2025a.
- Zhang, S., Fang, Q., Yang, Z., and Feng, Y. Llava-mini: Efficient image and video large multimodal models with one vision token. *arXiv preprint arXiv:2501.03895*, 2025b.
- Zhang, X., Gao, Z., Zhang, B., Li, P., Zhang, X., Liu, Y., Yuan, T., Wu, Y., Jia, Y., Zhu, S.-C., et al. Chain-of-focus: Adaptive visual search and zooming for multimodal reasoning via rl. *arXiv preprint arXiv:2505.15436*, 2025c.
- Zhao, K., Zhu, B., Sun, Q., and Zhang, H. Unsupervised visual chain-of-thought reasoning via preference optimization. In *ICCV*, 2025.
- Zheng, Z., Yang, M., Hong, J., Zhao, C., Xu, G., Yang, L., Shen, C., and Yu, X. Deepeyes: Incentivizing” thinking with images” via reinforcement learning. *arXiv preprint arXiv:2505.14362*, 2025.
- Zhu, J., Wang, W., Chen, Z., Liu, Z., Ye, S., Gu, L., Tian, H., Duan, Y., Su, W., Shao, J., et al. Internvl3: Exploring advanced training and test-time recipes for open-source multimodal models. *arXiv preprint arXiv:2504.10479*, 2025.
- Zhu, Y., Groth, O., Bernstein, M., and Fei-Fei, L. Visual7w: Grounded question answering in images. In *CVPR*, 2016.

A. Implementation Details

A.1. Datasets

For fair comparison with prior visual chain-of-thought methods, we adopt exactly the same training data as the corresponding backbone models.

Supervised Fine-Tuning (SFT). For supervised fine-tuning, we adopt the Visual-CoT dataset constructed following the protocol of Vis-CoT (Shao et al., 2024a). The dataset is built by collecting images and annotations from twelve publicly available datasets spanning five domains, including text/document understanding, fine-grained visual recognition, general visual question answering, chart understanding, and relation reasoning. These source datasets mainly consist of VQA and image captioning benchmarks, from which images and useful annotations such as question-answer pairs, captions, object bounding boxes, and object relations are reused. The data construction process involves both linguistic and visual annotation stages. For linguistic annotation, a large language model (GPT-4) is employed to generate or refine question-answer pairs and, where applicable, to produce intermediate reasoning steps. For visual annotation, task-relevant regions are identified to serve as visual chain-of-thought (CoT) grounding signals. In text-centric domains, such as TextVQA (Singh et al., 2019), DocVQA (Mathew et al., 2021), DUDE (Van Landeghem et al., 2023), SROIE (Huang et al., 2019), and InfographicsVQA (Mathew et al., 2022), OCR-based tools (e.g., PaddleOCR) are used to detect text regions, and the CoT bounding boxes are defined as regions containing words or sentences that directly support the answer. In fine-grained recognition tasks, bounding boxes corresponding to discriminative object parts or attributes are used to guide fine-grained visual reasoning. For general VQA and relation reasoning tasks, including Flickr30k (Plummer et al., 2015), Visual7W (Zhu et al., 2016), VSR (Liu et al., 2023), and GQA (Hudson & Manning, 2019), object-level annotations and scene graph information are leveraged. The visual CoT bounding boxes correspond to objects or regions that are explicitly involved in answering the question, such as spatially related objects or attributes specified in the query. In particular, for GQA, structured semantic annotations are used to identify the target objects and relations, enabling precise grounding of intermediate reasoning steps.

During SFT, each training example consists of an image, a question, a sequence of intermediate visual grounding steps represented by bounding boxes, and the final answer. The model is trained to jointly generate textual outputs and predict continuous bounding-box coordinates, allowing it to learn region-grounded visual reasoning under explicit supervision.

Reinforcement Learning (RL). For reinforcement learn-

ing, we adopt the same training data and protocol as DeepEyes (Zheng et al., 2025). Unlike supervised fine-tuning, the RL setting does not rely on any explicit intermediate bounding-box annotations. Instead, the model is optimized solely through outcome-level supervision, which better reflects practical scenarios where fine-grained visual grounding labels are unavailable.

The RL training data is constructed to emphasize tool-aware visual reasoning and consists of three complementary subsets: fine-grained visual search data, chart understanding data, and general reasoning data. The fine-grained subset is sampled from a portion of the V^* training set (Wu & Xie, 2024), focusing on high-resolution images and detailed perception tasks where localized visual inspection is critical for correct answering. The chart subset is drawn from ArxivQA (Li et al., 2024), which contains synthetic plots, diagrams, and structured graphical representations, significantly expanding the diversity of visual modalities beyond natural images. To further enhance reasoning diversity, some samples are incorporate from ThinkLite-VL (Wang et al., 2025d), which include multimodal questions requiring arithmetic reasoning, commonsense inference, and multi-step problem solving. Then a dedicated data selection pipeline is applied. First, question difficulty is estimated by prompting a strong vision-language model to generate multiple responses per question and measuring answer consistency; overly trivial or extremely difficult samples are filtered out. Second, original questions are reformulated into open-ended formats to better align with generative training objectives, and samples that cannot be reliably converted are discarded. Third, unverifiable instances are removed, including those with ambiguous questions, incorrect annotations, or unreadable visual content. Finally, chart data is exempted from this filtering step due to its inherent reliance on visual structure, while reasoning data is retained in its original form.

A.2. Evaluation Protocol

Inference Prompts. We employ two different prompt templates for reinforcement learning and supervised fine-tuning, respectively, reflecting their distinct training objectives and supervision signals. For reinforcement learning, we use a structured inference prompt that explicitly encourages step-by-step reasoning and conditional tool usage. The prompt instructs the model to first reason about the question, then optionally invoke the image zoom-in tool when fine-grained visual inspection is necessary, and finally produce the answer in a strictly defined format. This structured output separates reasoning, tool calls, and final answers, enabling reliable trajectory parsing and outcome-driven reward computation during policy optimization. For supervised fine-tuning, we adopt a localization-oriented prompt that explicitly asks the model to identify a task-relevant image region



Figure 6. More visualization results of bounding boxes. NV-CoT produces more accurate bounding boxes (shown in red) compared to the backbone model (shown in blue), demonstrating improved localization capability.

by predicting a bounding-box coordinate. The model is instructed to answer the question based on both the original image and the localized region. This prompt design encourages the model to learn explicit visual grounding under bounding-box supervision, strengthening the alignment between region selection and downstream reasoning.

RL Evaluating Prompt Template

Think first, call image_zoom_in_tool if needed, then answer.

Format strictly as:

*<think>...</think>
<tool_call>...</tool_call> (if tools needed)
<answer>...</answer>*

SFT Evaluating Prompt Template

Please provide the bounding box coordinate of the region that can help you answer the question better.

Answer the question based on the original image and local image.

B. More Visualization Results

In this section, we provide additional qualitative visualization results to further illustrate the behavior of our model under different visual reasoning scenarios. These examples complement the quantitative evaluations in the main paper and offer intuitive insights into how the model performs region grounding and integrates localized visual information during reasoning. Specifically, we visualize the predicted bounding boxes generated by the model for a variety of tasks, including fine-grained object recognition, spatial relation reasoning, and chart understanding. The results demonstrate that the model consistently identifies task-relevant regions that are closely aligned with the visual evidence required to answer the question, even in high-resolution images with cluttered backgrounds or small target objects.

C. LLM Usage Statement

ChatGPT was employed solely for minor editorial assistance, such as improving grammar and readability. The research ideas, methodology, experiments, and analysis were entirely developed and conducted by the authors without the use of LLMs.